Modeling and computation of fretting wear of structures under sharp contact

Hachmi Ben Dhia, Mohamed Torkhani

Modeling and computation of fretting wear of structures under sharp contact

Hachmi Ben Dhia[1, *, †] and Mohamed Torkhani[1,2]

[1]*Ecole Centrale Paris, MSSMAT, UMR ECP-CNRS 8579, 92295 Chatenay Malabry Cedex, France*
[2]*LaMSID—Laboratoire de Mcanique des Structures Industrielles Durables, UMR EDF-CNRS 2832, Clamart, France*

This paper is concerned with the modeling and simulation of the evolution of fretting wear of interacting solids submitted to cyclic loading and possibly undergoing large mechanical transformations. A Lagrangian formalism of the virtual work principle integrating significant worn volumes from the interacting solids is given. An extension of the Archard's wear model to the large transformations framework is developed and explained. Variational large transformations Lagrangian hybrid contact wear formulations are then derived. Wear explicit and wear implicit solution methodologies are described. A delocalized Archard's law is introduced to bound the wear of a structure under a corner or an edge of contact. Further, we resort to the multimodel Arlequin framework to capture efficiently wear concentrations as well as significant material removal due to wear, while enhancing the modeling flexibility and reducing the simulation costs of wear of structures, particularly thin ones. Our global methodology is assessed by some didactic numerical tests.

KEY WORDS: wear; finite transformations; extended Archard's law; sharp frictional contact; nonlocal wear law; Arlequin method

1. INTRODUCTION

Fretting wear refers to a very complex physical, chemical, and mechanical phenomenon that induces a damage of the near-interface zone of two interacting solids submitted to vibration or to cyclic loading. It leads to macroscopic cracks and/or to a material removal, creating in this case debris, sometimes labeled *third corps*. Wear is experienced by many engineering components (see e.g [1–3]), as well as biological ones (e.g. [4]). It might lead to their failure (see e.g. [5, 6]). In many industries, accurate wear prediction is important for the estimation of the remaining lifetime of critical components experiencing wear. Particularly in the nuclear industry, this issue is not only essential for a relevant safety diagnostic of existing nuclear infrastructures (see e.g. [7, 8]), but also for the design of components of the next nuclear plant generation.

From a computational point of view, wear prediction requires mainly the consideration of the following three items:

(i) a macroscopic wear model that describes correctly the involved phenomena;
(ii) an accurate contact modeling;

*Correspondence to: Hachmi Ben Dhia, Ecole Centrale Paris, MSSMAT, UMR ECP-CNRS 8579, 92295 Chatenay Malabry Cedex, France.
†E-mail: hachmi.ben-dhia@ecp.fr

(iii) an efficient numerical methodology for the simulation of a highly non-linear mechanical problem.

A large amount of work has been done on point (i). We refer to Meng and Ludema [9] for a significant overview. We also refer to [10, 11] and to a recent work by Stolz [12] (see also the references therein) for a thermodynamical approach of wear, considered as a moving discontinuity [13, 14].

In our work, although an extension to the finite transformations framework of the Archard's wear law is given and explained, item (ii) and item (iii), with special attention to the modeling and simulation of wear under sharp contact, are the main points of focus.

Although recognized as a crucial engineering issue, the numerical simulation of wear evolution is a rather recent computational research activity. This might well be linked to substantial numerical difficulties due to coupled non-linearities of contact conditions and wear criterion, to geometry changes of interacting worn solids and (last but not the least) to a missing simple and validated wear model [9].

Based on Archard's wear model [15], Goryacheva *et al.* [16] developed an analytical approach to investigate a model elastic two dimensional problem of fretting wear under partial slip. Based on the same wear model, Johansson [17] pioneered a finite element wear simulation in which contact is modeled by means of a penalty method. However, the latter is known to give interface fields quite sensitive to the penalty parameter, at least for reasonable choices of this parameter (namely not leading to ill-conditioning of the discrete mechanical system). An augmented-Lagrangian method (see e.g. [18–24]) all with a modified local Archard's model (e.g. [25]) is used by Stromberg [26]. These works were carried out under small perturbations hypotheses. Observe however that, for instance, a large mechanical transformations framework would be more appropriate for the simulation of wear of wire rope strands or more generally for cables (see e.g. [27] for a theoretical approach and [28] for a numerical one). Furthermore, the geometry change of significantly worn solids was not taken into account either in [17], or in [26, 29]. In [4], an extension of the Archard's model to the large transformations framework is developed. But the physical meaning of the additive decomposition of the deformation on which relies this extended (objective) model is not clear. The geometry change of the worn solids was developed by Podra and Andersson [30, 31] and further improved by Oqvist [32] and McColl *et al.* [25], by adapting the placement of the worn nodes of the mesh at each fictive time step of the wear process (considered in a quasi-static regime). Promising results were obtained by these authors. However, as reported in [25], the maximum wear depth control is mandatory to avoid instabilities. Moreover, without (costly) global remeshing, the adaptation of the placement procedure may lead to degenerated finite elements. For treatment of this issue, Paulin *et al.* [33] (see also [34]) suggest to confine the adaptation to the near interaction zone by selecting, from the beginning of the simulation, a set of nodes labeled the *wear box*. Note here that in [33], the authors use a simplified acceleration algorithm (inferred by experimental results) for the prediction of the evolution of wear to reduce the costs of simulation. A similar idea has been developed by McColl *et al.* [25] who suggested to use a refined local incompatible mesh in the critical interaction zone, coupled to the global mesh via the multipoint constraints to simplify the treatment of local surface adaptation. The possible distortion of elements due to this geometry adaptation is solved in Molinari *et al.* [35] via a precise continuous adaptive meshing (that might well become costly for complex 3D geometries).

In the (non-exhaustive) list of numerical papers on wear simulation reported above, very few of them have been dedicated to fine scales involved by the wear phenomenon. For instance, wear near a corner of contact has been considered in [36]. But the computational analysis of this simple but relevant problem was not fully investigated by the authors. A more accurate mesh adaptivity is used in [35] to approximate the problem. Moreover, the efficient wear modeling and simulation of thin elastic structures submitted to sharp contact, is in an even younger stage of development (see e.g. [37–40]).

The improved modeling and the numerical enhancement of the simulation of evolution of wear of elastic structures, particularly thin ones, submitted to the action of solids with sharp corners or edges of contact is the main goal of our paper. In particular, the multimodel Arlequin framework

[41–44] all with a simple nonlocal Archard's wear model, are shown to be effective engineering tools to address these issues.

An outline of the paper is the following: in the section following the introduction, a quasi-static Lagrangian *Virtual Work Principle* is written on the reference worn configurations of two solids undergoing large transformations, under frictional wearing contact. Section 3 is dedicated to the interface laws: the global classical Archard's wear law and its local version are recalled in Subsection 3.1. The extension of the Archard's wear law to the considered quasi-static large transformations framework is developed in Subsection 3.2, by using a conservation of worn mass. Equivalent settings of Signorini and Coulomb's friction laws [45, 46] integrating wear, are given in Subsections 3.3 and 3.4, respectively. By following in essence the works reported in [45, 46], the weak continuous Lagrangian formulation of the wear problem is developed in Section 4. Section 5 is dedicated to a description of the numerical strategy used to solve the problem defined in Section 4: explicit and implicit wear incremental schemes are presented and discussed. Moreover, a brief description of the finite element method and our special quadrature technique are briefly recalled. The wear modeling of plates under sharp contact is developed in Section 6, by using the multimodel and multiscale Arlequin framework. A delocalized wear model is introduced in Subsection 6.1 to tackle the singular behavior of wear under a corner or an edge of contact. Section 7 is devoted to the numerical solution of some quasi-static wear problems. A first bidimensional academic example consisting on a sharp rectangular elastic block acting on a larger elastic block is considered. This didactic test (similar to the one considered in [36] in 2D and in [26] in 3D) introduces a corner or an edge of contact. Several computations are carried out for this test to assess our theoretical investigations: first, we verify numerically that a local Archard's law leads to unbounded wear under the contact corner or edge (due to the singularity of the contact pressure) and show that the introduction of our simple nonlocal Archard's law bounds and stabilizes the wear profile in the critical contact zone. Second, we compare the numerical results obtained with a unilateral wear model (for which one solid is assumed to be not sensible to wear) to the ones derived with a bilateral wear model (wear of the two contacting solids). Third, the Arlequin framework is used to improve the flexibility of wear modeling and to reduce the simulation numerical costs. The influence of the change of geometry is also studied numerically. The last test is devoted to the feasibility of numerical simulation, in the Arlequin framework, of wear of a thin plate submitted to a sharp contact. The paper ends with some concluding remarks.

2. A LAGRANGIAN VIRTUAL WORK PRINCIPLE WITH MATERIAL REMOVAL

2.1. Notations, hypotheses, and problem position

We consider the problem of frictional wear-contact between two deformable solids B^1 and B^2. The classical Lagrangian localization of these two contacting solids relies upon their respective reference configurations. Because of material removal, taking into account finite wear requires a modification of the classical Lagrangian formalism. Indeed, as represented in Figure 1, the reference

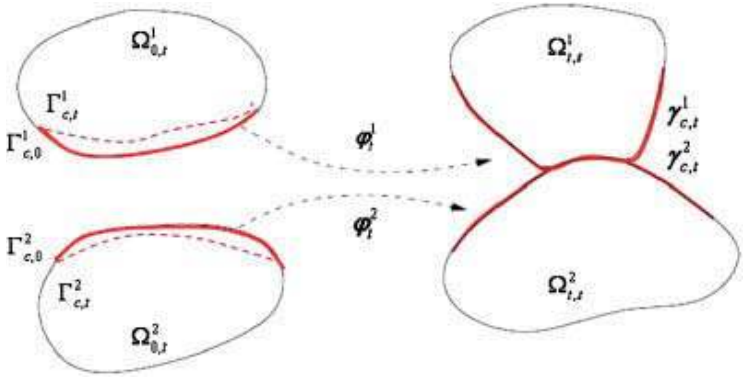

Figure 1. The contact/wear problem.

configurations of the worn solids become time-dependent. Let us notice $\Omega^1_{0,t}$ and $\Omega^2_{0,t}$ the (unknown) initial domains used to localize the worn solids at time t. Then, the current configurations of the solids B^1 and B^2 taking wear into consideration occupy the closures of the domains $\Omega^1_{t,t}$ and $\Omega^2_{t,t}$, defined, for each time t in the time interval $I=[0,T]$ of study of the system, by the following deformation (or motion) application (for $i=1,2$):

$$\begin{aligned} &\varphi^i_t : \Omega^i_{0,t} \to \Omega^i_{t,t} \\ &(\boldsymbol{p}^i) \mapsto \varphi^i_t(\boldsymbol{p}^i) \end{aligned} \tag{1}$$

The boundary of each domain $\Omega^i_{0,t}$ is partitioned into parts Γ^i_u (assumed to be fixed) where the displacements are prescribed, Γ^i_g (assumed also to be fixed) where the surface loads are given and $\Gamma^i_{c,t}$ the evolving 'reference' potential contact surface (at time t). The current positions of these boundary parts, denoted $\gamma^i_{u,t}$, $\gamma^i_{g,t}$, and $\gamma^i_{c,t}$, respectively, are assumed to constitute a partition of the boundary of $\Omega^i_{t,t}$.

In the remainder of the paper, the inertia terms and debris (third corps) will be neglected and the (fictive) time t will refer to an evolving loading. We shall be concerned with the quasi-static regime of the mechanical system. Further, body and boundary classical forces are omitted to simplify the notations. Only contact loads are considered.

2.2. Virtual work principle

Using classical notations, the *Virtual Work Principle*, combined with the action and reaction principle, reads as (for each fictive time $t; 0<t\leqslant T$):

Find $\boldsymbol{u}(t)=(\boldsymbol{u}^1(t),\boldsymbol{u}^2(t))\in \boldsymbol{CA}_{u,t}=\boldsymbol{CA}^1_{u,t}\times\boldsymbol{CA}^2_{u,t}, \boldsymbol{r}(t)\in\mathbf{R};\ \forall \boldsymbol{w}=(\boldsymbol{w}^1,\boldsymbol{w}^2)\in\boldsymbol{CA}_{u,t},$

$$G_{\text{int}}(\boldsymbol{u}(t),\boldsymbol{w})=G_c(\boldsymbol{r},\boldsymbol{w}) \tag{2}$$

where, for $i=1,2$, $(\boldsymbol{CA}^i_{u,t})_{i=1,2}$ denotes the space of kinematically admissible fields defined in $\Omega^i_{0,t}$, $\boldsymbol{u}^i$ is the displacement field,

$$G_{\text{int}}(\boldsymbol{u}(t),\boldsymbol{w})=\sum_{i=1}^{2} G^i_{\text{int}}=\sum_{i=1}^{2}\int_{\Omega^i_{0,t}} Tr[\boldsymbol{\Pi}^i(\boldsymbol{u}^i(t))(\nabla \boldsymbol{w}^i)^{\mathrm{T}}]\mathrm{d}\Omega^i \tag{3}$$

$$G_c(\boldsymbol{r},\boldsymbol{w})=\int_{\Gamma_{c,t}} \boldsymbol{r}.[\![\boldsymbol{w}]\!]\mathrm{d}\Gamma \tag{4}$$

with $\Gamma_{c,t}(=\Gamma^1_{c,t})$ being the potential 'slave' and reference contact surface, $\boldsymbol{\Pi}^i$ the first Piola–Kirchhoff stress tensor defined in $\Omega^i_{0,t}$ and $\boldsymbol{r}(\boldsymbol{p},t)=\boldsymbol{r}^1(\boldsymbol{p},t)=-\boldsymbol{r}^2(\bar{\boldsymbol{p}},t)$ the nominal vector-valued unknown density of contact forces experienced on $\Gamma_{c,t}$ by the worn solid B^1 from the worn solid B^2 (namely, $\boldsymbol{r}=\boldsymbol{\Pi}^1\boldsymbol{N}^1, \boldsymbol{N}^1$ referring to the unit outward normal vector to $\Gamma_{c,t}$). The (time depending) material point $\bar{\boldsymbol{p}}$ refers to a point belonging to the 'master' surface $\Gamma^2_{c,t}$ paired with the material point $\boldsymbol{p}$ of the 'slave' surface $\Gamma^1_{c,t}$ by using the classical closest point application [47] (see also [45, 48] for alternative pairing applications).

Moreover, in (4) and for $\boldsymbol{p}\in\Gamma_{c,t}$, $[\![\boldsymbol{w}]\!](\boldsymbol{p})=\boldsymbol{w}^1(\boldsymbol{p})-\boldsymbol{w}^2(\bar{\boldsymbol{p}})$ is the jump-like field defined on $\Gamma_{c,t}$.

System (2)–(4) has to be supplemented with material behavior laws, initial conditions, wear and contact laws. For the sake of simplicity, a hyperelastic behavior is assumed for the solids B^1 and B^2. That is:

$$\boldsymbol{\Pi}^i=\rho^i_0\frac{\partial W^i(\boldsymbol{F}^i)}{\partial \boldsymbol{F}^i} \tag{5}$$

where W^i is a local internal elastic energy per mass unit and $\boldsymbol{F}^i$ is the deformation gradient tensor. The solids are assumed to be initially free of residual stresses. As initial condition, we take:

$$\boldsymbol{u}^i(0) = \boldsymbol{u}^{i0} = 0 \quad \text{in } \Omega^i_{0,0} \tag{6}$$

where the reference initial configuration of B^i is known and denoted by $\Omega^i_{0,0}$.

3. CONTACT LAWS TAKING WEAR INTO ACCOUNT

The contact interface model taking wear into account constitutes the subject of this section. Global and local Archard's wear models are recalled in Subsection 3.1. Our extension of the Archard's local law to the large transformations framework is developed and explained in Subsection 3.2. Signorini's and Coulomb's contact laws, taking wear into account, are detailed in Subsections 3.3 and 3.4, respectively.

3.1. Archard's wear model

Archard [15] suggested a wear global model written in terms of worn volume loss. Actually, Archard's model relates wear to the dissipated frictional work. It reads as:

$$V^w = C P s \tag{7}$$

where V^w is the total worn volume, C the wear coefficient, P the applied normal load, and s the total accumulated sliding.

The local setting of the global Archard's model relates the local variation of the normal wear field of the interface, denoted here by w, to local interface fields. It reads as (see e.g. McColl *et al.* [25]):

$$\delta w = C \lambda \delta s \tag{8}$$

where C, λ, and δs are the local wear coefficient, the normal local pressure and the relative objective sliding (e.g. [23]), respectively.

3.2. An extension of the Archard's wear law to a large transformations framework

The law defined by (8) is valid under small mechanical perturbations hypotheses. In the large transformations framework considered here, we suggest that the current local variation of wear, pulled-back to the reference configuration, measured along the inward unit normal to the reference contact interfaces $\Gamma^i_{c,t}$ and denoted by δw^i_p (the indice p referring to the reference configuration) is given by the following extended local Archard's law:

$$\delta w^i_p = C^i J_{F^i} \lambda_p \delta s_p \quad \text{on } \Gamma^i_{c,t} \tag{9}$$

where J_{F^i} is the Jacobian of transformation φ^i, δs_p refers to the objective relative sliding pulled-back to the reference interface, λ_p is, at each reference material point $\boldsymbol{p} \in \Gamma_{c,t}$, the nominal normal contact pressure (measured along the unit normal to the current configuration at point $\boldsymbol{x} = \varphi(\boldsymbol{p}, t)$ of $\gamma_{c,t}$), and C^i are wear coefficients, providing (supposedly) agreement between theory and experiment (see e.g. [31, 32]). Observe that the variation of the reference normal wear depth is defined on $\Gamma^i_{c,t}$.

To explain (9), let us admit that the current wear variation δw^i_x is given by the Archard's local law, namely:

$$\delta w^i_x = C^i \lambda_x \delta s_x \quad \text{on } \gamma^i_{c,t} \tag{10}$$

Now, for $i = 1, 2$, denote by $(\delta_x S^i; \delta_p S^i)$, $(\delta_x m^{i,w}; \delta_p m^{i,w})$, and $(\delta_x V^{i,w}; \delta_x V^{i,w})$, the couple of infinitesimal surfaces, worn masses, and worn volumes, respectively, defined in the current and

reference configurations and associated to each other by means of the mechanical transformation φ^i. Denote by $(\rho_x^{i,w};\rho_p^{i,w})$ the couple of densities of mass. Then, the current and reference infinitesimal local worn masses are given by:

$$\delta_\alpha m^{i,w}=\rho_\alpha^{i,w}\delta_\alpha V^{i,w}\quad(\alpha=p\text{ or }x) \tag{11}$$

and, thanks to (10), the current infinitesimal local worn volume is given by:

$$\delta_x V^{i,w}=\delta_x S^i\,\delta w_x^i \tag{12}$$

If we admit that at each (fictive) time t and during the whole process (assumed to be quasi-static), the variation of the worn local mass is conserved in the following sense:

$$\delta_x m^{i,w}(\boldsymbol{x}^i)=\delta_p m^{i,w}(\boldsymbol{p}^i,t)\quad\text{for }\boldsymbol{x}^i=\varphi^i(\boldsymbol{p}^i,t),\quad \boldsymbol{p}^i\in\Gamma_{c,t}^i \tag{13}$$

which is a reasonable hypothesis, then the announced law can be established easily. Indeed, to get the infinitesimal variation of the wear pulled back to the reference configuration, first, we notice that:

$$\delta_p V^{i,w}=\delta w_p^i\,\delta_p S^i \tag{14}$$

Second, using all of (10)–(14), a local Lagrangian setting of the mass conservation $\rho_x^{i,w}=J_{F^i}\rho_p^{i,w}$, (assumed to hold for infinitesimal worn material), and the classical *Piola* relation, namely:

$$\lambda_p=\lambda_x\frac{\delta_x S^i}{\delta_p S^i} \tag{15}$$

we recover (9).

3.3. Signorini's unilateral model with wear

For notation simplification purpose, the subscript reference to the reference particle p is omitted in the sequel. Contact fields are defined by means of *Signorini* and *Coulomb* interface models. One of our formulation key points is the equivalent setting of the latter in terms of equations via the use of unknown Sign-like fields, defined on the assumed to be known potential contact surfaces (see [45, 46] and the references therein).

The *Signorini* contact laws read as:

$$d_n^w(\boldsymbol{p},t)\leqslant 0\quad\text{for }(\boldsymbol{p},t)\in\Gamma_{c,t}\times\mathrm{I} \tag{16}$$

$$\lambda(\boldsymbol{p},t)\leqslant 0\quad\text{for }(\boldsymbol{p},t)\in\Gamma_{c,t}\times\mathrm{I} \tag{17}$$

$$d_n^w(\boldsymbol{p},t)\lambda(\boldsymbol{p},t)=0\quad\text{for }(\boldsymbol{p},t)\in\Gamma_{c,t}\times\mathrm{I} \tag{18}$$

where $d_n^w(\boldsymbol{p},t)=[\![\varphi(\boldsymbol{p},t))]\!]\cdot\boldsymbol{n}(\boldsymbol{p},t)$ is the so-called normal signed distance, $\mathbf{n}(\boldsymbol{p},t)$ being the unit inward normal vector to the master surface at the point paired to $\boldsymbol{p}$ at time t. In the sequel, each vector-valued field $(*)$, defined on the contact interface is decomposed into its normal and tangential parts as $(*)=(*)_n\boldsymbol{n}+(*)_\tau$, with $(*)_n=(*)\cdot\boldsymbol{n}$.

Now, by introducing a Sign-like function, denoted by S_u^w, and by decomposing the nominal contact load as $\boldsymbol{r}=\lambda\boldsymbol{n}+\boldsymbol{r}_\tau$, (with $\lambda=\boldsymbol{r}\cdot\boldsymbol{n}$), the *Signorini* contact laws (16)–(18) taking wear into account, are transformed into the following multi-valued equalities that are equivalent to (16)–(18) (the explicit reference to $\boldsymbol{p}$ and t being omitted):

$$\lambda=S_u^w(\lambda-\rho_n d_n^w) \tag{19}$$

$$S_u^w=1_{\mathbb{R}^-}(\lambda-\rho_n d_n^w) \tag{20}$$

where, for a subset K of a space H, 1_K denotes the characteristic function of the set K (namely, for each $x\in\mathrm{H}$, $1_\mathrm{K}(x)=1$ if $x\in\mathrm{K}$ and $1_\mathrm{K}(x)=0$, otherwise) and ρ_n is a strictly positive real parameter, homogeneous to a string rigidity. (Observe that in (19), (20), the set K is the semi-axis of negative real numbers $\mathbb{R}^-$.)

3.4. Coulomb's frictional model with wear

In the same manner as for Signorini contact laws, we can prove that, by introducing a *Characteristic-Set* field S_f, *Coulomb*'s friction laws can be equivalently written as follows (see [46]):

$$(1-S_u^w)\boldsymbol{\Lambda}=\mathbf{0} \tag{21}$$

$$\boldsymbol{r_\tau}=\mu S_u^w \lambda \boldsymbol{\Lambda} \tag{22}$$

$$\boldsymbol{\Lambda}=S_f\boldsymbol{\Lambda}+(1-S_f)\left(\frac{\boldsymbol{\Lambda}+\rho_\tau[\![\boldsymbol{v}_\tau]\!]}{||\boldsymbol{\Lambda}+\rho_\tau[\![\boldsymbol{v}_\tau]\!]||}\right) \tag{23}$$

$$S_f=1_{B(0,1)}(\boldsymbol{\Lambda}+\rho_\tau[\![\boldsymbol{v}_\tau]\!]) \tag{24}$$

where S_u^w is defined by (20), $\boldsymbol{\Lambda}$ is the semi-Lagrange friction multiplier, $\boldsymbol{v}$ is the objective relative velocity field, μ is the friction coefficient, λ is the nominal local contact pressure, ρ_τ is a strictly positive real parameter, and $B(0,1)$ is the unit ball of $\mathbb{R}^d$ ($d=2,3$). Observe that when the contact is not active, namely when $S_u^w=0$, then there is no local friction load ($\boldsymbol{r}_\tau=\mathbf{0}$). When the contact is active, namely when $S_u^w=1$, then if $S_f=1$ no sliding is possible ($\boldsymbol{\Lambda}$ acts as a Lagrange multiplier) and if $S_f=0$, the sliding is possible (in this situation, $\boldsymbol{\Lambda}$ gives the sliding direction). Moreover, the infinitesimal sliding δs_p is equal to $\|[\![\boldsymbol{v}_\tau]\!]\|\delta t$.

4. WEAK CONTINUOUS LAGRANGE FORMULATION OF THE WEAR PROBLEM

By using (2)–(4), (19)–(20), and (21)–(24), a weak–strong hybrid formulation of the problem described above can be derived by following in essence the lines given in [46] and [45]. For each $t\in I$, it reads as:

Find $(\boldsymbol{u},\lambda,\boldsymbol{\Lambda},(w_p^i)_{i=1,2},S_u^w,S_f)\in \boldsymbol{CA}_u\times H_c\times \boldsymbol{H}_f\times(H_w^i)_{i=1,2}\times L^\infty(\Gamma_{c,0};\{0,1\})^2$; $\forall(\boldsymbol{w}^i,\lambda^*,\Lambda^*)$,

- *Virtual work principle*

$$\sum_{i=1}^{2} G_{\text{int}}^i(\boldsymbol{u}^i,\boldsymbol{w}^i)-\int_{\Gamma_{c,t}} S_u^w\lambda[\![w_n]\!]\mathrm{d}\Gamma$$
$$-\int_{\Gamma_{c,t}}\mu S_u^w\lambda\left[S_f\boldsymbol{\Lambda}+(1-S_f)\frac{\boldsymbol{\Lambda}+\rho_\tau[\![\boldsymbol{v}_\tau]\!]}{\|\boldsymbol{\Lambda}+\rho_\tau[\![\boldsymbol{v}_\tau]\!]\|}\right][\![\boldsymbol{w}_\tau]\!]\mathrm{d}\Gamma=0 \tag{25}$$

- *Signorini–Archard weak law*

$$-\frac{1}{\rho_n}\int_{\Gamma_{c,t}}[\lambda-S_u^w(\lambda-\rho_n d_n^w)]\lambda^*\,\mathrm{d}\Gamma=0 \tag{26}$$

- *Coulomb–Archard weak law*

$$\frac{1}{\rho_\tau}\int_{\Gamma_{c,t}}\mu S_u^w\lambda\left\{\boldsymbol{\Lambda}-\left[S_f(\boldsymbol{\Lambda}+\rho_\tau[\![\boldsymbol{v}_\tau]\!])+(1-S_f)\frac{\boldsymbol{\Lambda}+\rho_\tau[\![\boldsymbol{v}_\tau]\!]}{\|\boldsymbol{\Lambda}+\rho_\tau[\![\boldsymbol{v}_\tau]\!]\|}\right]\right\}\boldsymbol{\Lambda}^*\,\mathrm{d}\Gamma$$
$$+\int_{\Gamma_{c,t}}(1-S_u^w)\boldsymbol{\Lambda}\boldsymbol{\Lambda}^*\,\mathrm{d}\Gamma=0 \tag{27}$$

- *Sign-like fields*

$$S_u^w=1_{\mathbb{R}^-}(\lambda-\rho_n d_n^w) \tag{28}$$

$$S_f=1_{B(0,1)}(\boldsymbol{\Lambda}+\rho_\tau[\![\boldsymbol{v}_\tau]\!]) \tag{29}$$

- *Archard's type local wear law*

$$\delta w_p^i(t)=C^i J_{F^i}(t)\lambda(t)\delta s_p(t)\quad\text{on }\Gamma_{c,t}^i\quad i=1,2 \tag{30}$$

- *Initial conditions*

$$\boldsymbol{u}^i(0)=0 \quad \text{in } \Omega^i_{0,0}=\Omega^i_0, \quad i=1,2 \tag{31}$$

$$w^i_p(0)=0 \quad \text{on } \Gamma^i_{c,0}=\Gamma^i_c, \quad i=1,2 \tag{32}$$

where

- G^i_{int} is defined by (3),
- $\boldsymbol{CA}_u$, H_c, $\boldsymbol{H}_f$, and $(H^i_w)_{i=1,2}$ are the spaces of kinematically admissible displacement fields, contact Lagrange multipliers, friction (semi-) Lagrange multipliers, and wear fields, respectively.

Observe that for the sake of clarity of notations, the explicit reference to time, both for the unknown and virtual fields and for the unknown domains, was omitted.

For the numerical solution of the problem (25)–(32), the main difficulty when compared to classical contact problems, is related to the unknown evolution of the potential reference contact surface position, due to wear. The following section focuses mainly on the latter issue.

5. NUMERICAL SOLUTION ALGORITHM

Friction loads depend on the relative tangential velocity field and require an incremental (fictive) time strategy. The wear variation law is more intricate: it is an evolution law that leads to the alteration of the interacting solids, changing consequently the reference domains occupied by these solids. The incremental form of the wear problem (25)–(32) has to rigorously take into account this geometry variation. In practice and due to complexity of wear problems, more or less simplified incremental formulations have been developed. Here, we distinguish two main incremental formulations: an explicit and an implicit one. For this, we consider the time interval $\boldsymbol{I}=[0,T]$ to be a collection of non-overlapping subintervals $[t_k,t_{k+1}]$, i.e. $\boldsymbol{I}=\bigcup_{k=0}^{n_T}[t_k,t_{k+1}]$, with $0=t_0<t_1\cdots<t_k<t_{k+1}<\cdots<t_{n_T+1}=T$. We denote by $\Delta t_k=t_{k+1}-t_k=\Delta t$ the time step (chosen here to be constant for simplicity) and by $(*)_k$ the approximation of the field $(*)(t_k)$ at time. Moreover, we assume that, at a time step t_k, for $k=1,n_T$, the displacement field $\boldsymbol{u}_{k-1}$, the wear field $w^i_{p,k-1}$ and consequently the placement of the potential reference contact surface $\Gamma_{c,k-1}$ are known.

5.1. Wear explicit algorithm

In this strategy, the reference slave contact surface $\Gamma_{c,t}$, at time snap-shot t_k, $(k>0)$, is frozen to its (known) position at time t_{k-1}. This leads to the following *wear explicit* incremental large transformations elastic frictional contact problem:

Find $(\boldsymbol{u}_k,\lambda_k,\boldsymbol{\Lambda}_k,((w^i_p)_k)_i=1,2),S^w_{uk},S_{fk})\in \boldsymbol{CA}_{u,k-1}\times H_{c,k-1}\times \boldsymbol{H}_{f,k-1}\times (H^i_{w,k-1})_{i=1,2}\times L^\infty(\Gamma_{c,k-1};\{0,1\})^2$;

$$G_{\text{int}}(\boldsymbol{u}_k,\boldsymbol{w})+G_{\text{cont}}(\lambda_k,\boldsymbol{u}_k,\boldsymbol{w})+G_{\text{fric}}(\boldsymbol{\Lambda}_k,\lambda_k,\boldsymbol{u}_k,\boldsymbol{w})=0 \quad \forall \boldsymbol{w}\in \boldsymbol{CA}_{u,k-1} \tag{33}$$

$$G^{\text{weak}}_{\text{cont}}(\lambda_k,\boldsymbol{u}_k,\lambda^*)=0 \quad \forall \lambda^*\in H_{c,k-1} \tag{34}$$

$$G^{\text{weak}}_{\text{fric}}(\boldsymbol{\Lambda}_k,\lambda_k,\boldsymbol{u}_k,\boldsymbol{\Lambda}^*)=0 \quad \forall \boldsymbol{\Lambda}^*\in \boldsymbol{H}_{f,k-1} \tag{35}$$

with

$$G_{\text{int}}(\boldsymbol{u}_k,\boldsymbol{w})=\sum_{i=1}^{2}\int_{\Omega^i_{0,k-1}} Tr[\Pi^i_k(\nabla \boldsymbol{w}^i)^{\mathrm{T}}]\mathrm{d}\Omega^i \tag{36}$$

$$G_{\text{cont}}(\lambda_k,\boldsymbol{u}_k,\boldsymbol{w})=-\int_{\Gamma_{c,k-1}} S^w_{uk}g^w_{nk}[\![w_n]\!]\mathrm{d}\Gamma \tag{37}$$

$$G_{\text{fric}}(\boldsymbol{\Lambda}_k, \lambda_k, \boldsymbol{u}_k, \boldsymbol{w}) = -\int_{\Gamma_{c,k-1}} \mu S_{uk}^w \lambda_k \left\{ S_{fk}\boldsymbol{\Lambda}_k + (1-S_{fk})\frac{\boldsymbol{g}_{\tau k}}{\|\boldsymbol{g}_{\tau k}\|} \right\} \cdot [\![\boldsymbol{w}_\tau]\!] \mathrm{d}\Gamma \tag{38}$$

$$G_{\text{cont}}^{\text{weak}}(\lambda_k, \boldsymbol{u}_k, \lambda^*) = \int_{\Gamma_{c,k-1}} -\frac{1}{\rho_n}\{\lambda_k - S_{uk}^w g_{nk}^w\}\lambda^* \, \mathrm{d}\Gamma \tag{39}$$

$$G_{\text{fric}}^{\text{weak}}(\boldsymbol{\Lambda}_k, \lambda_k, \boldsymbol{u}_k, \boldsymbol{\Lambda}^*) = \int_{\Gamma_{c,k-1}} \frac{-\mu S_{uk}^w \lambda_k}{\underline{\rho}_\tau} \left\{ \boldsymbol{\Lambda}_k - \left(S_{fk}\boldsymbol{\Lambda}_k + (1-S_{fk})\frac{\boldsymbol{g}_{\tau k}}{\|\boldsymbol{g}_{\tau k}\|} \right) \right\} \boldsymbol{\Lambda}^* \, \mathrm{d}\Gamma$$

$$+ \int_{\Gamma_{c,k-1}} (S_{uk}^w - 1)\boldsymbol{\Lambda}_k \boldsymbol{\Lambda}^* \, \mathrm{d}\Gamma = 0 \tag{40}$$

where

$\Pi_k^i = \Pi^i(\boldsymbol{u}_k^i)$
$g_{nk}^w = \lambda_k - \rho_n d_{nk}^w$
$d_{nk}^w = [\![\varphi_k]\!] \cdot \boldsymbol{n}_k$
$\Delta \boldsymbol{u}_{\tau k} = \boldsymbol{u}_{\tau k} - \boldsymbol{u}_{\tau(k-1)}$
$S_{uk}^w = 1_{\mathbb{R}^-}(g_{nk}^w)$
$\boldsymbol{g}_{\tau k} = \boldsymbol{\Lambda}_k + \underline{\rho}_\tau [\![\Delta \boldsymbol{u}_{\tau k}]\!]$
$S_{fk} = 1_{B(0,1)}(\boldsymbol{g}_{\tau k})$
$\underline{\rho}_\tau > 0$

Observe that the augmented Lagrangian-like parameter $\underline{\rho}_\tau$ is homogeneous to the parameter ρ_τ (appearing in the continuous formulation, defined by (25)–(32)), divided by a (fictive) time.

This is now a frictional large transformations elastic contact problem that we solve by means of the finite element method, a collocation method (namely a particular quadrature procedure for the contact terms [45]) and an algorithm detailed in [46]. Once this discrete non-linear problem has been solved, wear is adjusted as follows:

$$w_{nk}^i = w_{n(k-1)}^i + C^i J_{F_k^i} \lambda_k \| [\![\Delta \boldsymbol{u}_{\tau k}]\!] \| \tag{41}$$

As long as the final time snap-shot t_T is not reached, the potential reference contact surface is consequently updated and a next time step is solved.

The main drawback of this strategy is that it may lead to numerical instabilities if the wear variation during one step is too large (e.g. [25]), which is a classical limitation of general explicit approaches.

Before describing a wear implicit approach, let us observe that the described wear explicit algorithm can be simplified (especially for infinitesimal wear) by freezing the reference potential contact interface to its initial position for all the time steps. With this strategy, the wear field can be considered as an internal variable (calculated by numerical integration of the wear law) and used to correct the signed normal distance for the contact problems.

5.2. Wear implicit algorithm

Contact forces are known to be very sensitive to the interacting surfaces profiles. Thus, even a small error on the estimation of the worn surface profiles, due to the use of the approximate explicit wear algorithm, may significantly change the final worn volumes. In this subsection, we develop an implicit wear algorithm. With this second strategy, the *wear explicit algorithm*, developed in Subsection 5.1, is used iteratively in each current time step t_k to adjust, till convergence, the current slave reference contact surface. More precisely, the following scheme is used:

- *step* 1: (initialization) set $\Gamma_{c,k}^0 = \Gamma_{c,k-1}$;
- *step* 2: (solution) solve problem (33)–(40) with $\Gamma_{c,k}$ replaced by $\Gamma_{c,k}^0$, exactly as described in the *wear explicit algorithm*;

- *step* 3: (update) compute $\Gamma^1_{c,k}$ by using the incremental wear law;
- *step* 4: (test) compare $\Gamma^1_{c,k}$ to $\Gamma^0_{c,k}$;
- *step* 5: (decision) if the two geometries compare to within a given small tolerance, then take $\Gamma_{c,k} = \Gamma^1_{c,k}$ and stop the iterations for the time t_k. Otherwise, replace $\Gamma^0_{c,k}$ by $\Gamma^1_{c,k}$ and go to step 2.

These algorithms are used for the solution of some academic tests in the final numerical section and let us mention here that, for a significantly important number of loading cycles, we have also tested the acceleration approximate idea suggested by McColl *et al.* [25] to reduce the computational costs of wear evolution simulation.

6. MODELING OF SOME SPECIAL WEAR PROBLEMS WITHIN THE ARLEQUIN FRAMEWORK

One point of focus of this paper is the modeling and simulation of evolution of wear under sharp contact. In case where one of the two contacting solids presents a sharp corner or edge of contact, the contact pressure experienced by the other solid becomes singular in the critical contact zone. With the local Archard's model, this leads to a local infinite wear. This situation is obviously not acceptable from a physical point of view. To correct the model, a delocalized Archard's law is suggested in Subsection 6.1.

However, even when a delocalized wear law is used (with a relatively small delocalization distance), the contact pressure keeps on varying abruptly in the critical contact zone. To capture this pressure concentration with sufficient accuracy, one can resort to refinement techniques, such as the h-adaptivity finite elements technique (see e.g. [35]). However, for three-dimensional complex interfaces, this relevant global refinement technique might well become costly.

In Subsection 6.2, we show how the multimodel and multiscale Arlequin framework can be easily used to handle this issue. Furthermore, we show how this framework can also be used to introduce the delocalized wear law of Subsection 6.1 only where it is needed, namely in the near corner or edges of contact zones, in order to reduce the simulation costs.

6.1. A nonlocal Archard's wear model

Let us recall here the local wear model we developed in Subsection 3.2:

$$\delta w^i_p = C^i J_{F^i} \lambda_p \delta s_p \quad \text{on } \Gamma^i_{c,t} \tag{42}$$

The delocalization operator we suggest here consists in replacing in (42) the local normal nominal contact load λ at a point $\boldsymbol{p}$ by an average $\widetilde{\lambda}$ of λ over the intersection of the potential contact slave surface $\Gamma_{c,t}$ with a disk (in 3D) or a segment (in 2D), contained in the slave surface $\Gamma_{c,t}$, of radius β and centered in $\boldsymbol{p}$. This leads to the following delocalized wear law:

$$\delta w^i_p = C^i J_{F^i} \widetilde{\lambda} \delta s_p \quad \text{on } \Gamma^i_{c,t} \tag{43}$$

This delocalized wear law is discussed numerically in the last section and we notice that, instead of the simple averaging technique, one can use a delocalization based on a molifying technique, namely a convolution of the normal pressure with a gaussian-like function, also called a coarse graining technique (which will be tested in a forthcoming work). In all cases, the delocalization radius has to be calibrated numerically. (It could also be related to a kind of *Representative Surface Element* when available). Here, to test the feasibility of the approach, we have given a fixed arbitrary numerical value to the radius β in our numerical simulations.

6.2. The Arelquin framework for contact and wear problems

The Arlequin method [41, 42] (see also [43, 44, 49]) is a global–local type partition of model framework which allows concurrent multiscale and multimodel analyses. This method has already

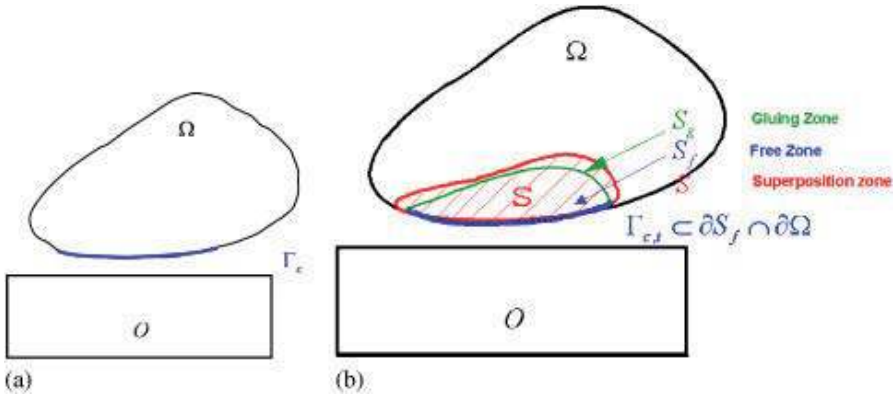

Figure 2. (a) Model problem and (b) Arlequin coupling.

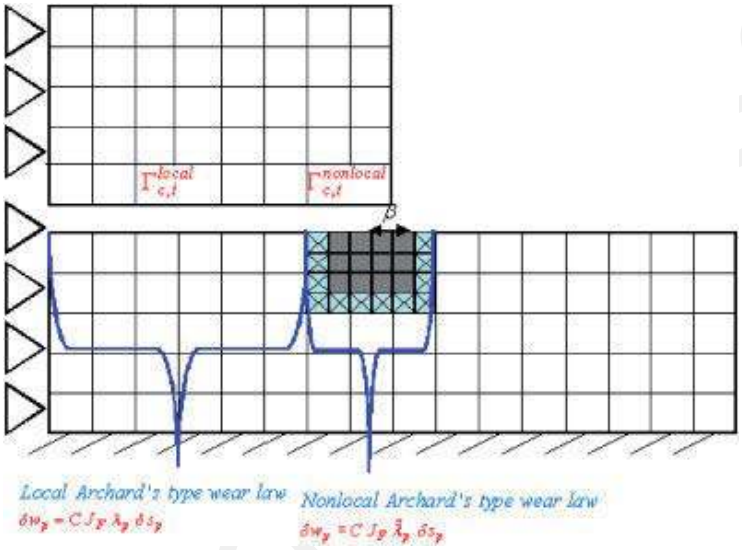

Figure 3. Multi-wear laws in the Arlequin framework.

been used in many mechanical fields (e.g. [43, 44, 50–52]). For unilateral contact problems, it was first used in [53]. It is applied here to sharp wear problems. The Arlequin method consists in (i) superimposing a local model to a global one in a zone of interest (say S) of the latter, (ii) distributing the mechanical energies between the super-imposed zones by means of partition of unity functions, and (iii) gluing the models in a part S_g of S by using Lagrange multipliers, the remainder of S being the free zone. Figure 2(b) shows how this can be done for a contact problem, shown by Figure 2(a). Observe that the complementary domain of S_g in S is denoted by S_f (as free zone in which the two models are superposed with no coupling). The main advantage of the method is that it allows to enrich, with enhanced flexibility and thus reduction of simulation costs, an existing global model to take into account the local mechanical features of the problem in hand that are not resolved by the global model.

To illustrate the application of the method to sharp wear contact problems, we consider the bidimensional case of two solids, represented in Figure 3. In the near corner of contact zone, a refined patch is superimposed to the coarsely meshed solid located at the bottom. The gluing or coupling zone is marked by crosses in the figure.

Two main features of the Arlequin method can be noticed here. The first is that the patch can be meshed much more finely than the global model (whose mesh can be kept fixed) in order to capture the contact pressure concentration near the corner of contact. Second, in the free zone of the patch S, the contact between the two solids is taken into account by means of the interaction of the patch surface with the upper solid. Further, the wear law used in this local part of the contact interface, (denoted by $\Gamma_{c,t}^{\text{nonlocal}}$ in Figure 3) can be the nonlocal one, defined by (43), in order to

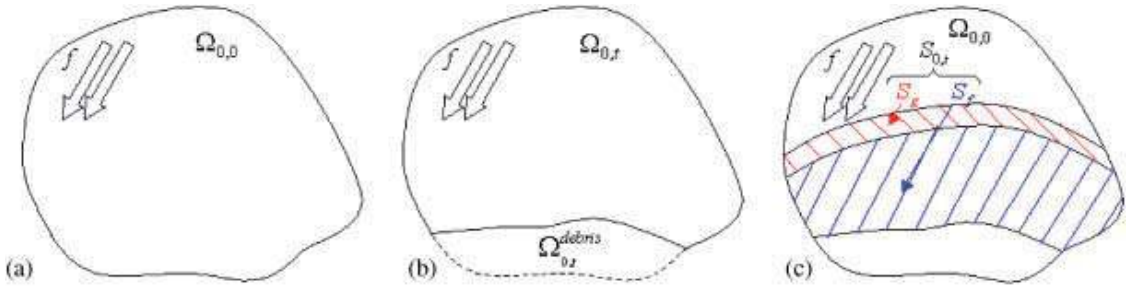

Figure 4. (a) Unworn solid; (b) Worn solid; and (c) Arlequin models superposition.

bound the wear field in this zone. At the same time, the local wear law (42) can be used in the remainder of the contact interface $\Gamma_{c,t}^{\text{local}}$, (with $\overline{\Gamma}_{c,t}^{\text{local}} \cup \overline{\Gamma}_{c,t}^{\text{nonlocal}} = \overline{\Gamma}_{c,t}$ and $\Gamma_{c,t}^{\text{local}} \cap \Gamma_{c,t}^{\text{nonlocal}} = \emptyset$). In the latter part, the contact pressure is regular.

Another important numerical application of the Arlequin method concerns the treatment of contact problems with finite wear amounts. Actually, when the material removal from solid surfaces due to wear actions is relatively small, the only correction of the contact gap field might be sufficient to simulate the wear evolution front (as mentioned at the end of Subsection 5.1). But, when the wear amounts are no more negligible, this simplified modeling may suffer precision. A remeshing (eventually adaptive remeshing) can be used to account for physical material loss. Let us explain here how this issue can be addressed, with enhanced flexibility (and thus reduction of simulation costs) within the Arlequin modeling framework. (Observe here that an alternative approach, based on the Level Set method of Osher and Sethian [54] can also be used. A comparison of both techniques will be done in a forthcoming work.)

Let us consider the sound (unworn) solid $\mathscr{B}$, occupying the closure of the initial domain $\Omega_{0,0}$ (see Figure 4(a)). Let us suppose that the solid $\mathscr{B}$ experiences the removal of a part $\mathscr{B}^{\text{debris}}$ of its material, that occupied the closure of a sub-domain $\Omega_{0,t}^{\text{debris}}$ of $\Omega_{0,0}$ (see Figure 4(b)). The worn solid occupies now the closure of the domain $\Omega_{0,t}$. In order to model the worn solid living in the closure of $\Omega_{0,t}$, we superimpose to the sound (unworn) domain $\Omega_{0,0}$ a (copy of a) significantly smaller subdomain $S_{0,t}$ of $\Omega_{0,0}$, whose geometry reflects the material loss (cf. Figure 4(c)). Then, following the ideas of the Arlequin approach, we:

- duplicate the mechanical fields in $S_{0,t}$,
- let the mechanical energies be shared in $S_{0,t}$ by the superposed models,
- couple the two states in a gluing sub-zone of $S_{0,t}$ (denoted S_g in Figure 4(c))

to derive an Arlequin problem (see e.g. [44]).

Note that, since the superposition zone $S_{0,t}$ is chosen in such a manner that it lies in the sound solid $\mathscr{B}$ and since we neglect the *debris*, then the (Arlequin) weight α we affected to $\Omega_{0,t}^{\text{debris}}$ is $\alpha \approx 0$. Thus, the portion of the internal global work, defined in $\Omega_{0,t}^{\text{debris}}$, corresponding to the neglected lost material, is almost zero.

Now, in terms of Finite Element discretization of the Arlequin problem, while keeping a global unchanged FE model, defined in the initial domain (and, consequently, using a fixed global coarse mesh to approximate the regular part of the solution), we insert, at some time increments for which worn volume is considered to be significant, a local geometrically adapted Arlequin patch, i.e. a local model whose geometry is updated according to the wear scar.

Observe here that whereas the methodology of [34] uses a single global mechanical field-based formulation and (cumbersome) multipoint constraints to glue the super-imposed 'wear patch', the present methodology uses one local and one global mechanical fields and *ad hoc* coupling operators in the Arlequin framework.

The relevance of the Arlequin approach in dealing with all these special wear problems is assessed in the following section through simple numerical tests that illustrate:

(1) the importance of delocalization of the wear law to correct the singularity of Archard's local wear profiles near contact corners or edges;

(2) the feasibility of local unilateral/bilateral geometry update (without any change of the global sound mesh) to account for material removal due to wear;
(3) the multimodel computing of wear of a thin structure, under sharp contact conditions.

7. NUMERICAL RESULTS

The problem of two interacting blocks is chosen to demonstrate the feasibility and relevance of the methodology developed in the previous sections. The two-dimensional version of this problem, depicted in Figure 5, consists in a $10 \times 0.5\,\mathrm{cm}^2$ elastic block, fixed at its left edge, clamped on the bottom and unilaterally constrained at its top edge by a sharp elastic tool which is 1000 times stiffer than the elastic block. The tool is subjected to the surface loads f and F, where f is a given normal pressure acting on its top edge and F is a shearing cyclic load acting on its right edge, with an amplitude of 10 daN/mm (see the right part of Figure 5). These loading conditions lead to fretting wear of the first block. The block and the tool are approximated by 64×10 and 32×10 four-nodes bilinear finite elements, respectively. The potential contact surface at the top of the block is approximated by 16 1D linear finite elements to approximate the contact forces. The trapezoidal quadrature rule is used. Consequently, the contact integration points coincide with the nodal displacement points of the contact surface. This particular choice of the nodes located on the boundary Γ_{ch} is the well-known node-on-facet strategy which is accurate for compatible interacting meshes. Observe that, for accuracy, more involved quadrature rules are mandatory for general incompatible contact interface meshes [45, 53]. Each shear cycle is discretized by $n_{incr} = 4$ '(fictive) time steps' or increments. Linearized and homogeneous elasticity is assumed. The parameters and material properties used in the finite element computations are:

- Young's modulus for the elastic block $E = 210\,\mathrm{GPa}$
- Poisson's ratio $\nu = 0.3$
- friction coefficient $\mu = 0.3$
- constant wear coefficient $C = 1.0 \times 10^{-11}\,\mathrm{Pa}^{-1}$

In the sequel, several variants of this numerical test are achieved:

(i) The first test aims to stress the mesh-dependency and unboundness of the wear profile induced by the locality of Archard's model in the vicinity of the contact corner and assesses the engineering effectiveness of the wear delocalization in the Arlequin framework.
(ii) The point of focus of the second test is the illustration, in the Arlequin framework, of the feasibility of (unilateral) wear geometry update of the 'slave' contacting surface by means of geometrically adapted local patches integrating the worn volumes.

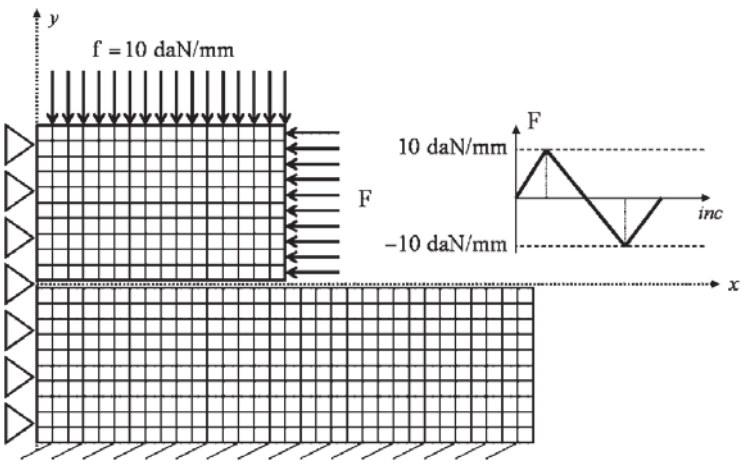

Figure 5. A 2D elastic block subjected to given normal and shear cyclic loads.

(iii) The third test shows the differences between the consideration of unilateral and bilateral wear models, combined with the wear-related geometry update.
(iv) The fourth and last test considers the fretting wear for a mixed 3D/plate (bi)model.

7.1. Effectiveness of the nonlocal Archard's law

The same fretting test as in Figure 5 is used here to show the engineering effectiveness of the delocalized wear law. The potential contact surface corresponds to the interval $\Gamma_{\text{ch}} = \{(x, 0); x \in [0, 5](\text{in cm})\}$. Two different FE models are considered, a classical coarse one and a second using a fine Arlequin patch superposed to the coarsely meshed elastic block:

- For the classical coarse FE model, 32×10 bilinear finite elements are used for the tool and 64×10 bilinear finite elements are used for the elastic block,
- For the second FE model, a $1.625\,\text{cm} \times 0.2\,\text{cm}$ Arlequin rectangular patch, composed of 24×16 bilinear finite elements, is superimposed to the lower elastic block. The top edge of the patch is centered at the corner of contact (as indicated in Figure 3).

Local and delocalized Archard's-like wear laws are used for both models. The length of the nonlocal wear zone is $l = 1\,\text{cm}$ (i.e. $\Gamma_{c,h}^{\text{local}} = [0, 4]\,\text{cm}$ and $\Gamma_{c,h}^{\text{nonlocal}} = [4, 5]\,\text{cm}$). The parameter β is equal to $0.3125\,\text{cm}$.

The results plotted in Figure 6 show how the use of the nonlocal Archard's law stabilizes the results obtained with the local Archard's law.

In order to confirm the stabilization induced by the nonlocal wear law, we consider, for the second finite element model described above, three increasingly refined meshes of the Arlequin patch, (each refinement consisting in subdividing uniformly each rectangular element of the previous mesh into four rectangular elements), while conserving the same nonlocal wear zone $\Gamma_{c,h}^{\text{nonlocal}} = [4, 5]\,\text{cm}$, the same delocalization radius $\beta = 0.3125\,\text{cm}$ and the same coarse finite element model.

Figure 7 depicts the wear scars corresponding to the three FE models when using either a local or a nonlocal wear law in the contact interface of the patch. We clearly observe that the wear profiles corresponding to the local Archard's model are mesh-dependent, whereas those corresponding to the nonlocal wear law are stabilized, despite the narrower refinement in the neighborhood of the contact corner.

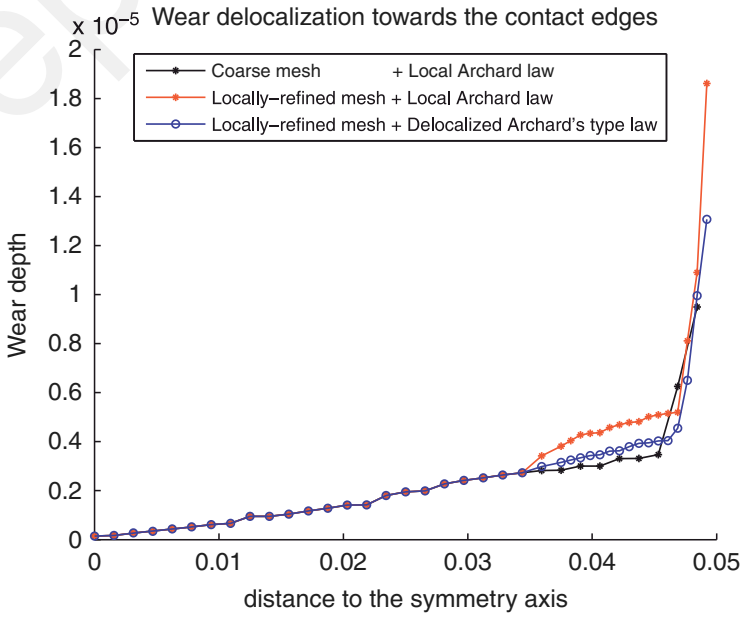

Figure 6. Comparison of wear results obtained with a local and a nonlocal Archard's wear law.

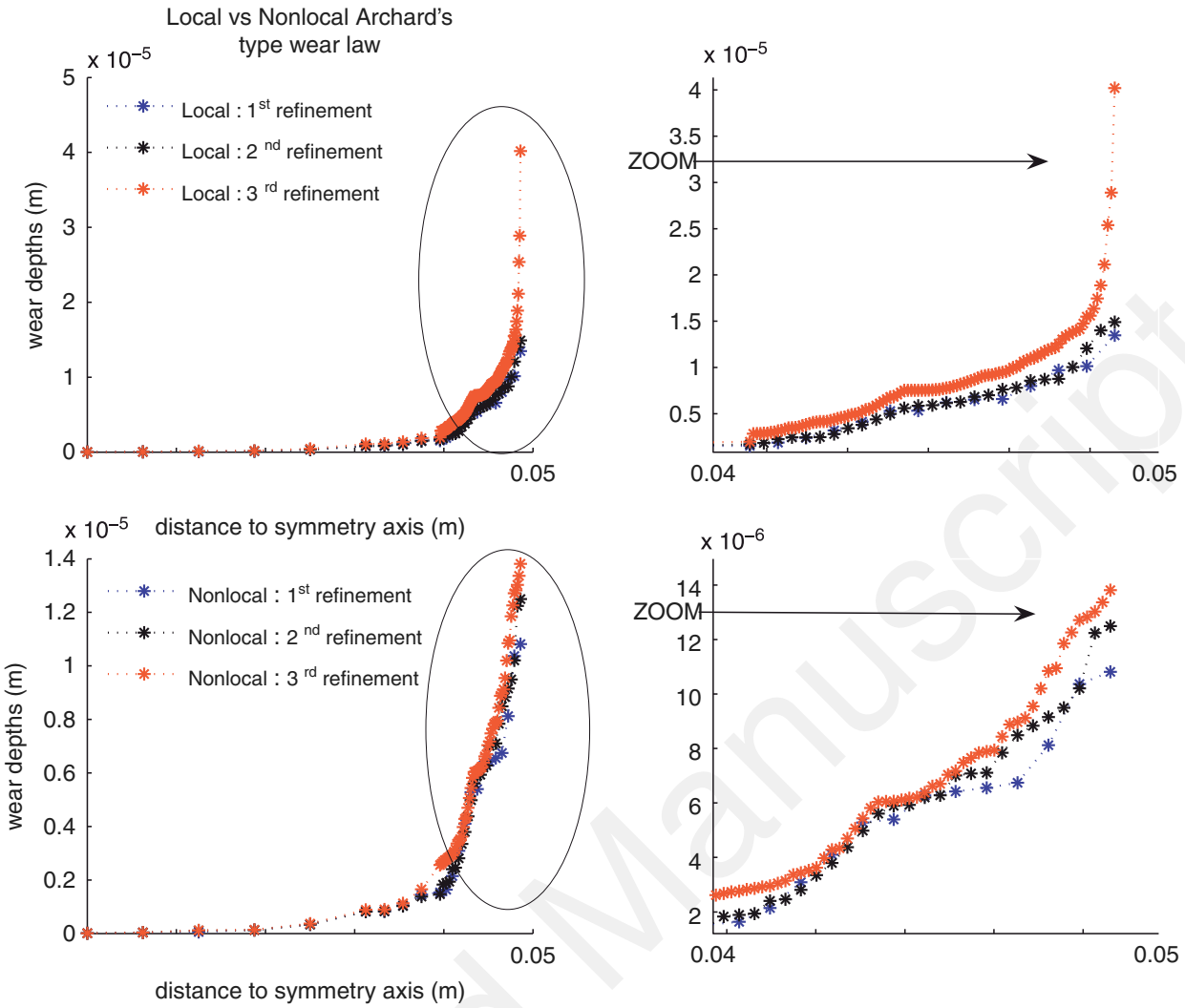

Figure 7. Stabilized wear profiles with respect to the mesh for the delocalized wear law.

7.2. *Simulation of significant worn volumes*

In this section, we exemplify the potential of the Arlequin framework to simulate finite fretting wear problems, with significant worn volumes requiring for accuracy a material removal from the initial interacting solids. Here, the wear-related geometry update procedure is unilaterally applied to the lower 'slave' block contacting surface of the numerical test represented by Figure 5. For this test, the implicit version of the developed geometry adaptation procedure has been applied up to $N_t = 10000$ fretting cycles. We have used the acceleration approximate procedure of McColl *et al.* [25] with an acceleration factor $k = 100$. Each 'representative' fretting cycle is discretized into four increments.

The wear depth and normal contact pressure distributions resulting from numerical simulations with and without unilateral wear-related geometry correction are plotted in Figure 8. It is worth mentioning that the Arlequin-based geometry update leads to sharper stress gradients and deeper wear depths at the leading contact edge. This means that the nonphysical updating geometry procedure is not conservative.

Among other reasons explaining the local sharp stress variations mentioned above, one can point out the fact that the tool is not wearing out and that its geometry is not updated. In the following subsection, we consider bilateral wear and bilateral-related geometry update.

7.3. *Unilateral vs bilateral wear and geometry update*

We consider the same model problem of Figure 5 and we assume that the tool is wearing out even if the amount of material lost from this (almost) rigid block is relatively small when compared

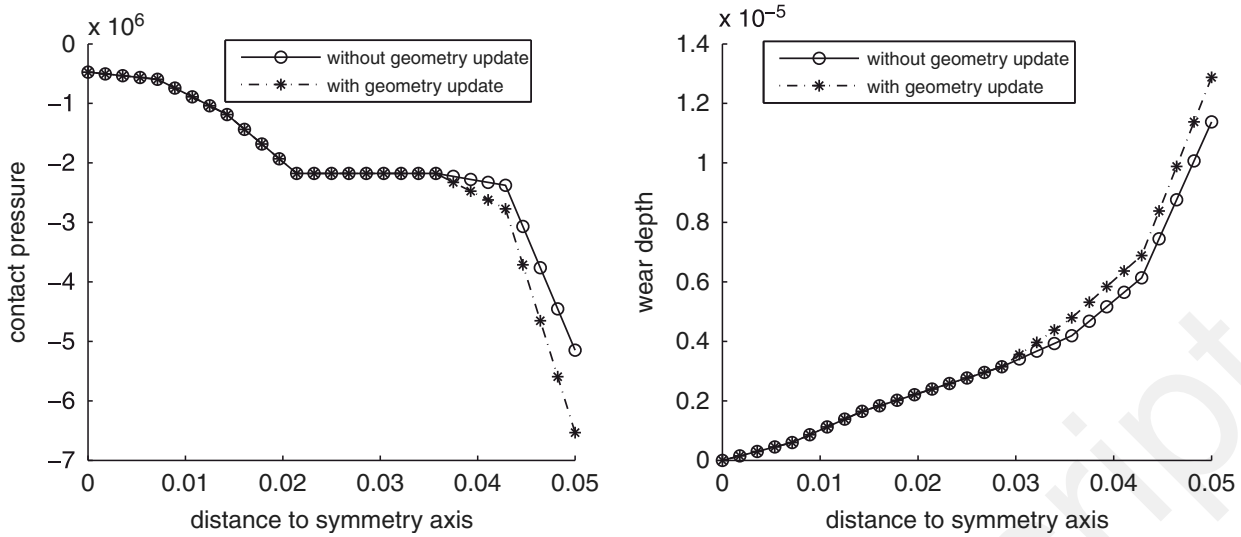

Figure 8. Wear depth and normal contact pressure distributions with and without unilateral wear-related geometry update.

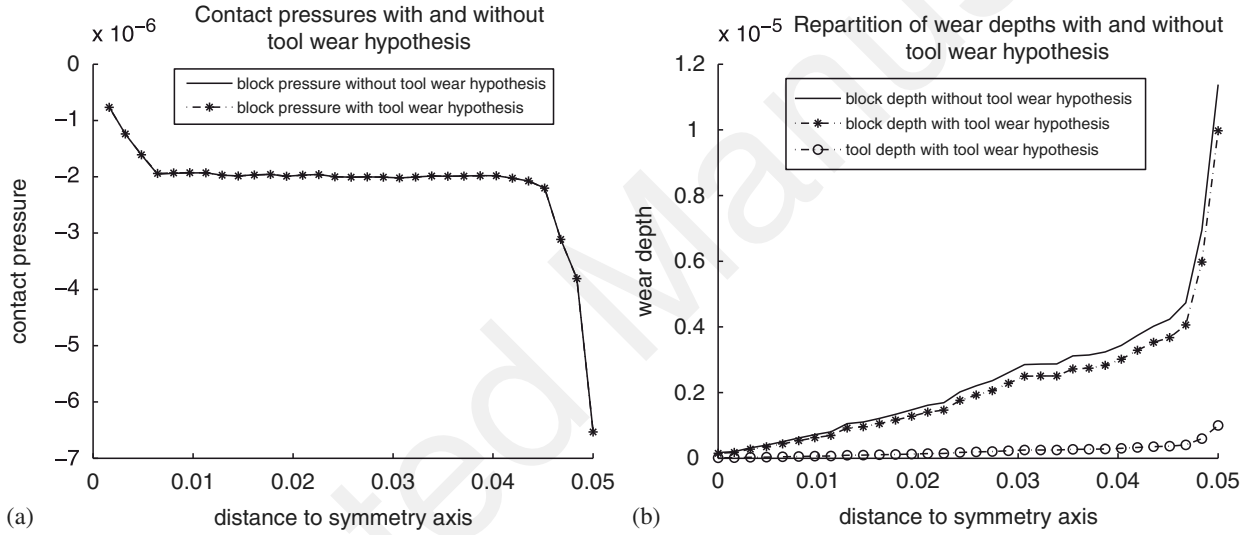

Figure 9. Influence of tool wear and geometry update: (a) contact pressure distribution on the elastic block and (b) wear depth profiles on the elastic block and the sharp tool.

to the elastic block. The wear coefficients used in Archard's wear laws for the elastic block and the tool are $C^1 = 1.0 \times 10^{-11}\,\mathrm{Pa}^{-1}$ and $C^2 = 1.0 \times 10^{-12}\,\mathrm{Pa}^{-1}$, respectively. Two tests are carried out. In the first one, wear is calculated only on the 'slave' elastic block (unilateral wear) whereas, in the second, wear is calculated on both 'slave' elastic block and 'master' tool (bilateral wear). The results in Figure 9(b) show that under bilateral wear assumption the tool is actually worn out. As for the elastic block, wear patterns are donut-shaped with large values at the contact corners. Contact pressures corresponding to unilateral and bilateral wear are depicted in Figure 9(a). At the leading contact corner, one can notice that bilateral wear modeling gives weaker wear gradients when compared to the ones obtained with unilateral wear modeling. The appreciable 'flattening' effect observed on the wear profiles can be directly related to the rounded edges of the local geometrically adapted patches and to the inherent increase of the surface conformity yielding to the wear processes.

7.4. Wear of thin structures

Engineering thin structures may be subjected to wearing contact actions that are so localized that their analysis by means of thin structure FE models becomes locally irrelevant.

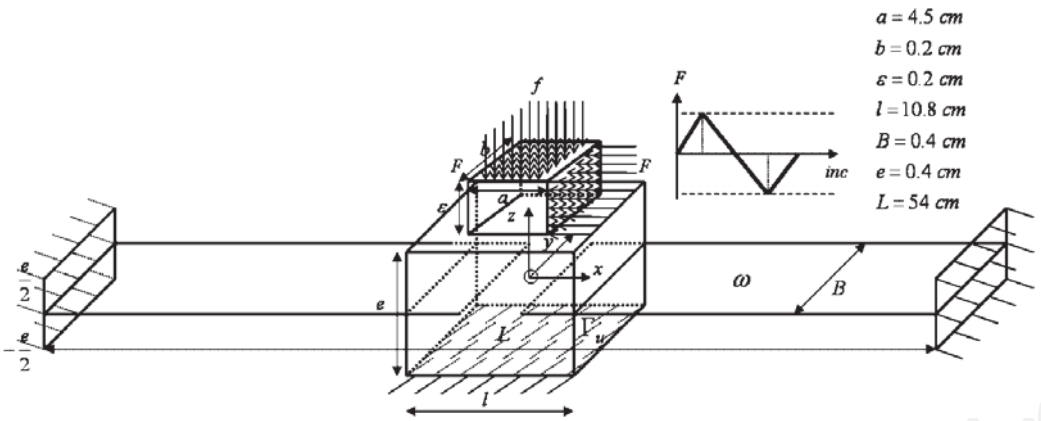

Figure 10. Fretting wear with a mixed plate/3D Arlequin (bi)model.

The potential of the Arlequin method to couple a global thin shell model and a local 3D patch has been reported in [44]. Here, we show a feasibility test of computation of a problem of wear of a thin structure under sharp contact conditions. For this, we consider a thin plate occupying the closure of the domain $\omega\times]-e/2, e/2[$, where $\omega=]-L/2, L/2[\times]-B/2, B/2[$ and e are the mid-surface and the thickness of the plate, assumed to be clamped on two opposite lateral faces, free on the other two lateral faces, clamped on a part of its bottom face and submitted to the wear action of a sharp tool at its top face (see Figure 10 for details and data).

The tool is submitted to a cyclic loading as in the previous tests. To take into account the local effects of the tool, especially near the edges of contact, an Arlequin bimodel is created. It is composed of a local 3D solid model, superimposed to a global thin structure model and partially glued to it. The local 3D solid model is located under the tool and interacts with it through wearing contact conditions (see Figure 10). This problem is then discretized and solved by means of the numerical methodology described in the numerical section. In particular, the mid-surface ω of the global plate model is meshed with 50 uniform rectangular elements. The Arlequin 3D patch is meshed in a first computation with $18\times7\times8$ eight nodes brick elements and $12\times4\times4$ eight nodes brick elements are used for the sharp indenter for all the computations.

Figure 11 depicts contact pressures and wear depths on the slave contact surface of the solid patch, after 10, 20, and 30 cycles.

It is worth noticing a qualitative similarity with results reported in [26] for a different 3D wear problem consisting of an elastic block unilaterally constrained to a rigid support and submitted to similar loads as the ones considered here.

Figure 12 represents the restriction to the $(x, 0, z)$ plane of the wear profiles obtained with an equivalent complete 3D (mono)model and the mixed Arlequin (bi)model. One can underline the similarity between the obtained wear profiles.

Finally, Figure 13 shows that the resulting mixed plate/3D Arlequin (bi)model can display significant through-the-thickness stresses.

Nevertheless, we are aware that the modeling of this problem (but also the others involving singularities) has to be pushed forward to derive more accurate numerical solutions. The results shown by Figure 14 were derived for the same mechanical problem by using a second mesh for the patch (obtained by subdividing uniformly each brick element of the first mesh of the patch into eight brick elements). The results given in Figure 15 were derived by using a third mesh obtained from the second one by using the same refinement procedure. The wear depths on the effective contact surface obtained with the three FE models after 30 cycles are compared to each other in Figure 16. One can observe that a reasonable convergence is reached there where the wear field is regular but not in the near contact edges or contact corner zones. This is more clear in Figure 17 where the wear is represented along particular cross sections of the contact surface. Observe for instance that in the central part of Figure 17 (wear along the cross-section $y=0$ of the contact surface) the three curves are quasi-superposed, where the wear field is regular.

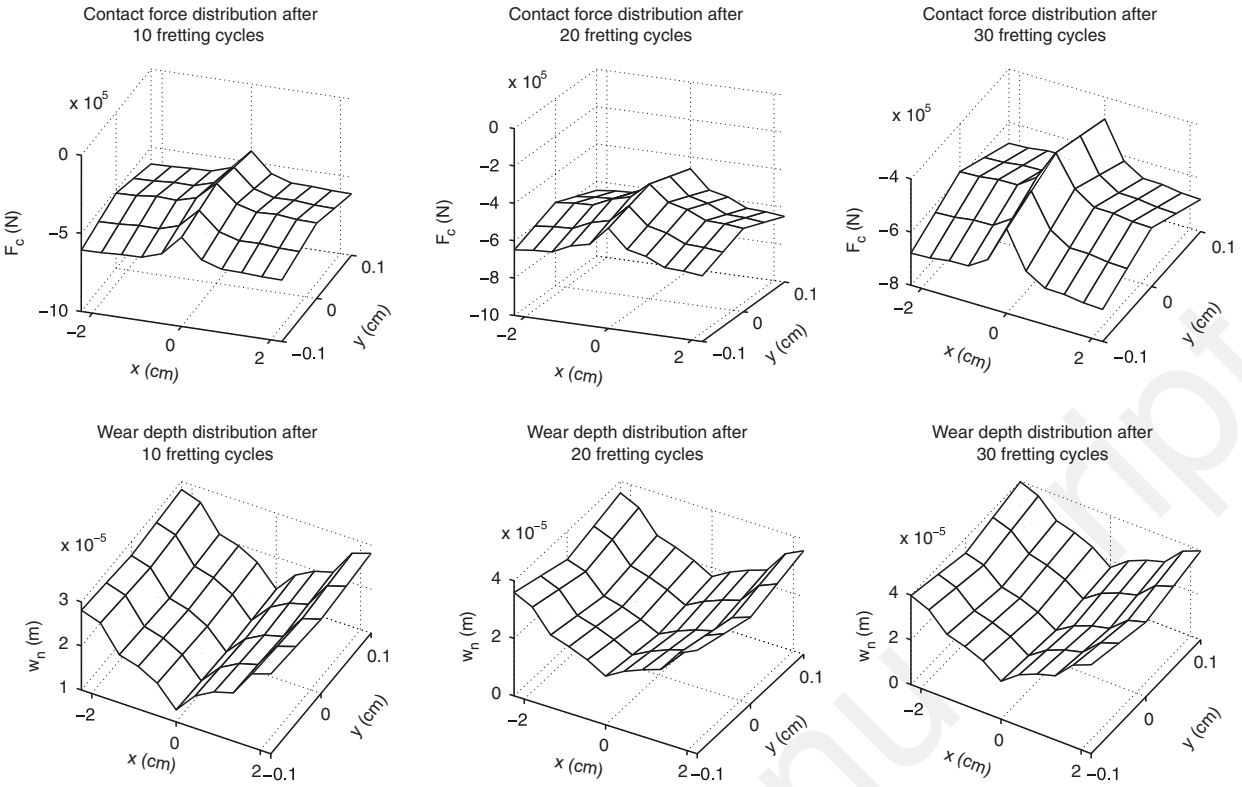

Figure 11. Contact pressure and wear depth distributions on the contacting surface after 10, 20, and 30 fretting cycles.

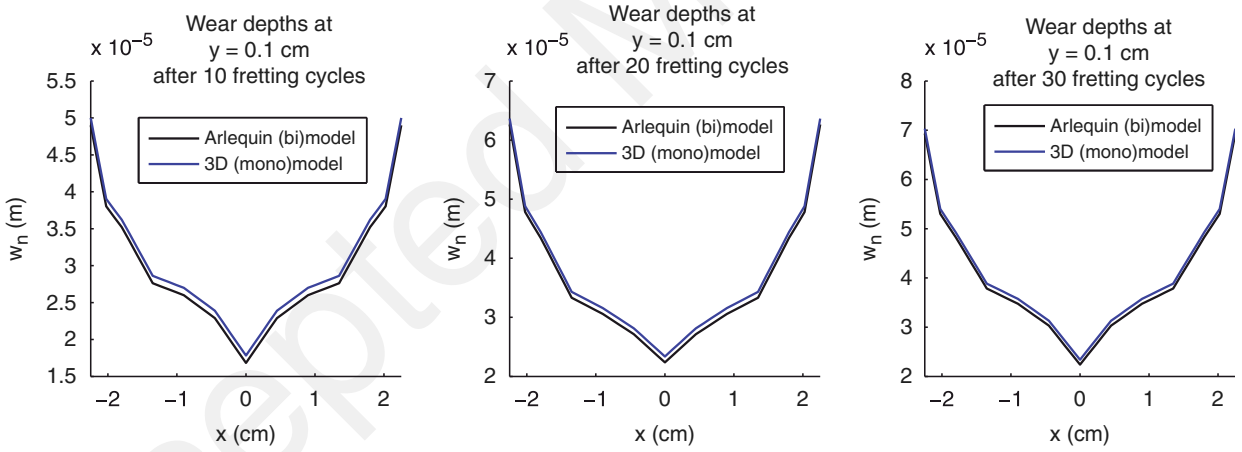

Figure 12. Comparison of wear depth patterns between the fine 3D (mono)model and the Arlequin mixed plate/3D (bi)model.

As for 2D wear problems, a simple way of stabilization of the pressure and consequently of the wear fields in the singular zones could be a delocalization of the wear model. Another more involved and classical approach consists in using h-p-adaptive strategies (e.g. [55]), although we believe that one has also to refine the physical models themselves near the edges and corners of contact.

8. CONCLUDING REMARKS

A hybrid Lagrangian continuous formulation of the problem of wear of interacting structures submitted to cyclic loading, is developed in this paper in a large transformations framework. Using a conservation of infinitesimal worn material mass, or volume hypothesis, (seemingly original)

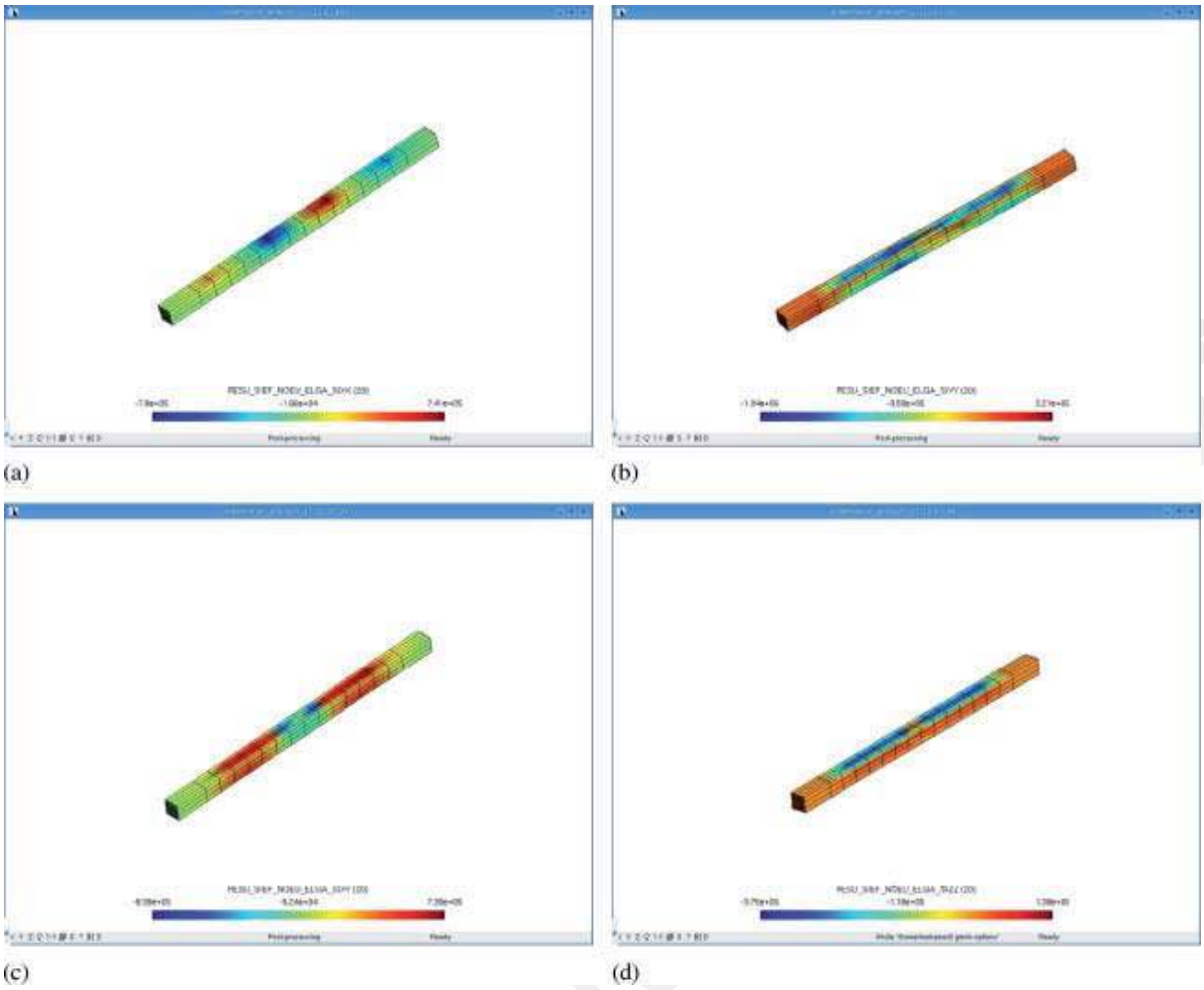

Figure 13. (a) σ_{xx}; (b) σ_{yy}; (c) σ_{xy}; and (d) σ_{zz}.

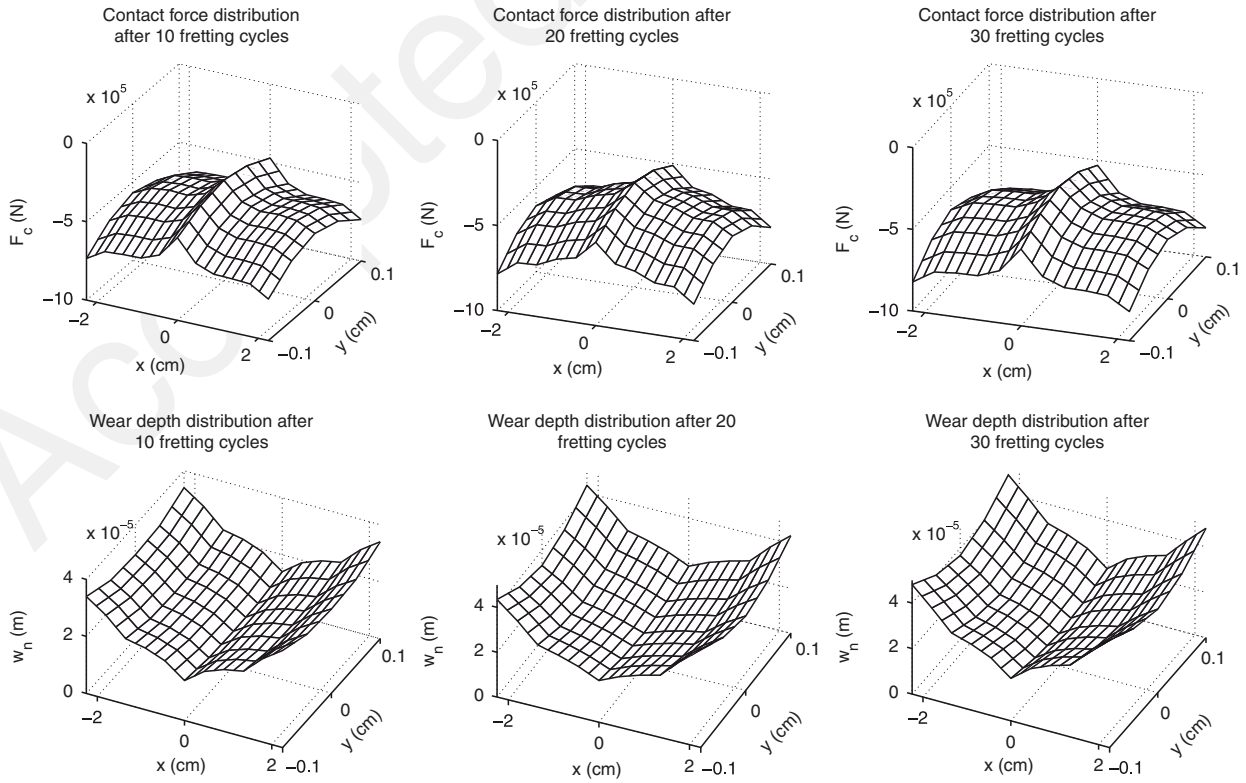

Figure 14. Contact pressure and wear depth distributions on the contacting surface after 10, 20, and 30 fretting cycles with a first refinement.

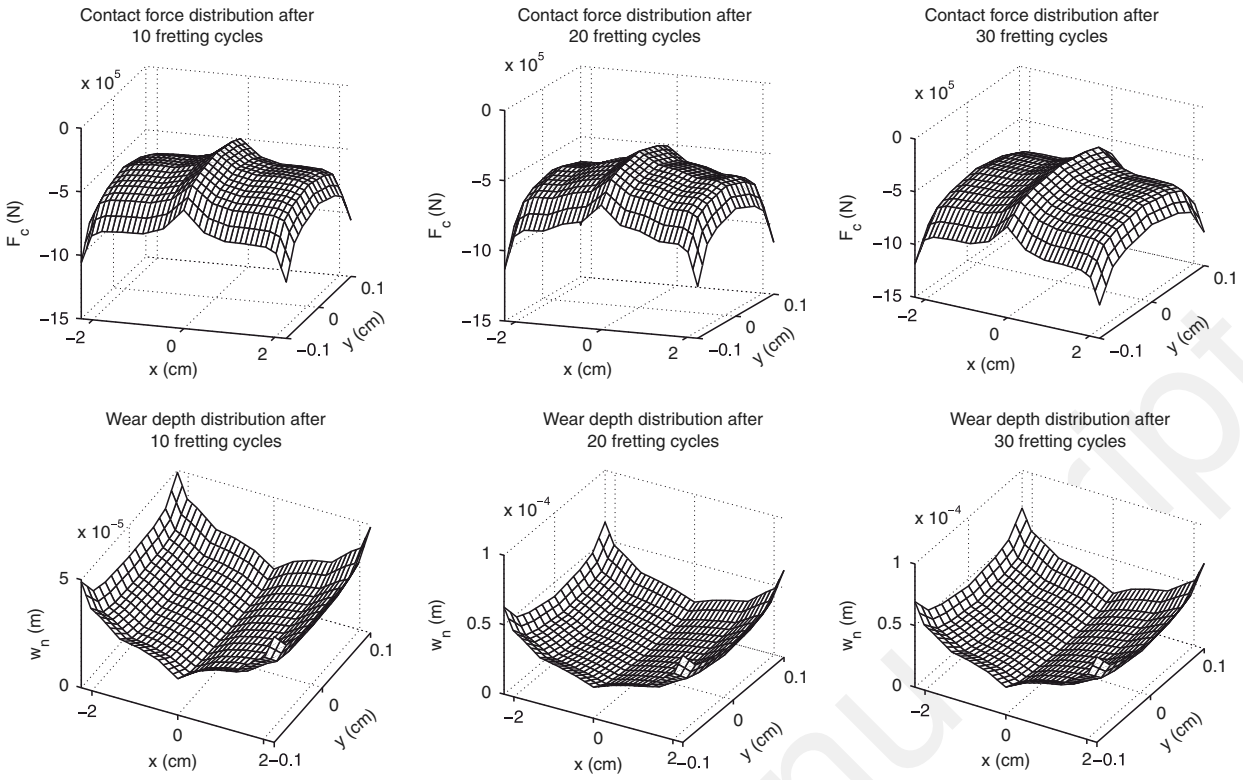

Figure 15. Contact pressure and wear depth distributions on the contacting surface after 10, 20, and 30 fretting cycles with a second refinement.

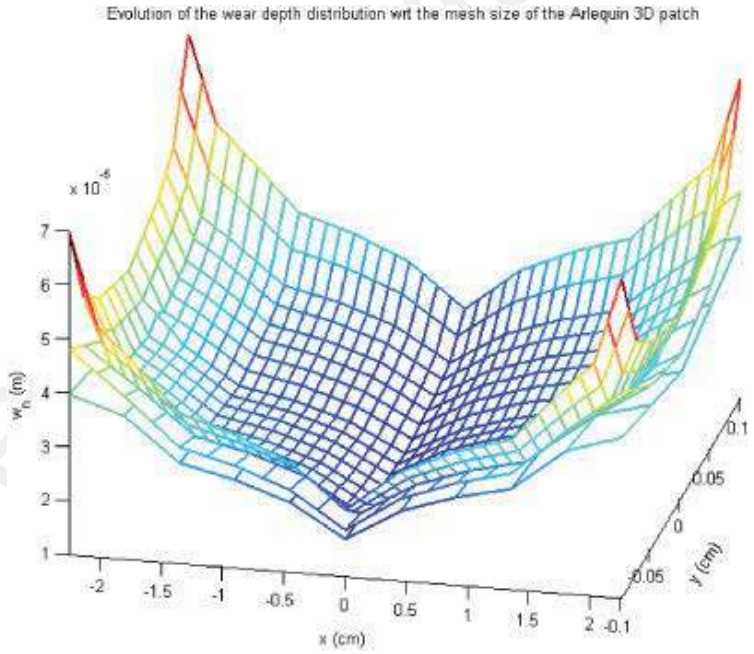

Figure 16. Comparison of wear depths distributions for the three meshes on the contacting surface after 30 fretting cycles.

extensions of the local Archard's wear law to large transformations are suggested, explained and integrated in the hybrid frictional wearing contact problem. A numerical solution strategy is detailed. In particular, a wear explicit and a wear implicit integration schemes are detailed. One of the main goals of the paper is to address wear of structures under sharp contact. To achieve this task, a simple nonlocal wear law is suggested. Its effectiveness to stabilize the wear profiles is illustrated through a simple but relevant example. Furthermore, the Arlequin framework is shown to be an appropriate one for the treatment of some particular wear problems with flexibility and

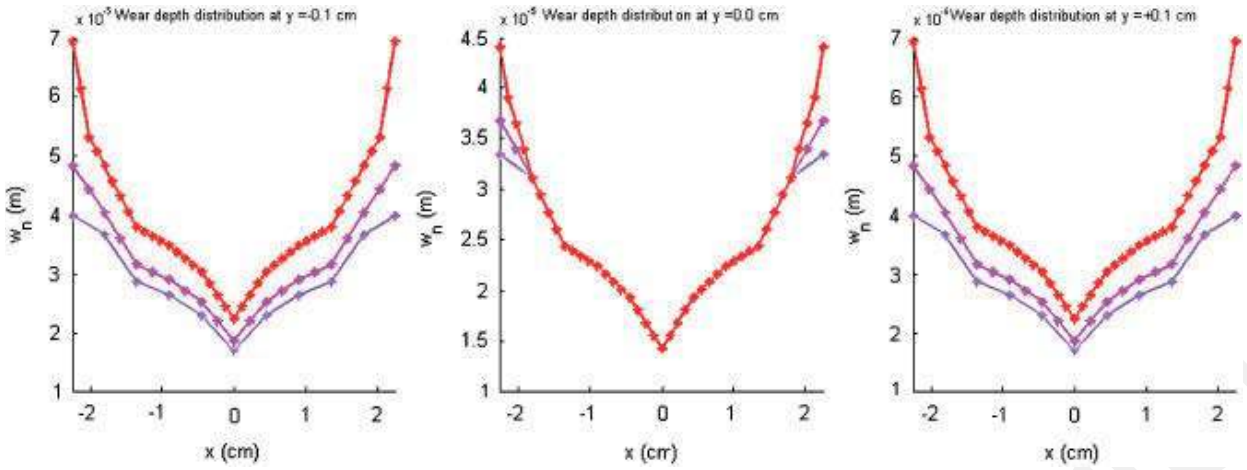

Figure 17. Comparison of wear depths for the three meshes on three cross sections ($y=-0.1\,\text{cm}$, $y=0\,\text{cm}$, and $y=0.1\,\text{cm}$).

reduction of costs of the simulations. Two engineering questions, in particular, are addressed in this framework:

- the fretting simulations taking into account the contact geometry change due to material removal by wear via geometrically adapted Arlequin patches;
- the fretting wear of thin structures by using the multimodel character of the Arlequin method.

The cyclic localized stresses in cyclic sliding contact give rise to localized contact plastic deformations and/or to local fatigue failure. The macroscopic elasticity assumed herein in a first analysis can not provide a precise description of these severe local damage mechanisms that might cause micro-cracks initiation and macro-crack creation (see e.g. [36, 56]). In the future work, we will focus on a better integration of more complex physical behaviors to provide a more accurate elaboration of wear in critical zones coupled to macroscopic wear models in regular zones. The multiscale modeling Arlequin framework should help us to address these challenging issues.

Finally, let us also mention that the use of Level Set methods with thermodynamically based wear laws to propagate wear constitutes another horizon for a future work.

ACKNOWLEDGEMENTS

The support of Électricité de France is gratefully acknowledged.

REFERENCES

1. Gassner E. The value of surface-protective media againt fretting corrosion on the basis of fatigue strength tests. *Laboratorium for Betriebsfestigkeit TM19/67*, 1967.
2. Johnson RL, Bill RC. Fretting in aircraft turbine engines. *NASA TM X-71606*, 1974.
3. Buch A. Fatigue and fretting of pin-lug joints with and without interference fit. *Wear* 1977; **43**:9–16.
4. Jourdan F. Numerical wear modeling in dynamics and large strains: application to knee joint protheses. *Wear* 2006; **261**:283–292.
5. Waterhouse RB. Fretting fatigue. *International Materials Review* 1992; **37**:77–97.
6. Hills DA, Nowell D. *Mechanics of Fretting Fatigue*. Kluwer Academic Publishers: Dordrecht, 1994.
7. Fisher NJ, Chow AB, Weckwerth MK. Experimental fretting wear studies of steam generator materials. *Journal of Pressure Vessel Technology* 1995; **117**:312–320.
8. Lee CY. Theoretical analysis for studying the fretting wear problem of steam generator tubes in a nuclear power plant. *Nuclear Engineering and Technology* 2005; **37**:201–206.
9. Meng HC, Ludema KC. Wear models and predictive equations: their form and content. *Wear* 1995; **181–183**: 443–457.
10. Dragon-Louiset M, Stolz C. A thermodynamical approach to contact wear. *Comptes Rendus de l'Académie des Sciences, Paris* 1999; **t.327, Ser. II**:1275–1280.
11. Dragon-Louiset M. On a predictive macroscopic contact-sliding wear model based on micromecanical considerations. *International Journal of Solids and Structures* 2001; **38**:1625–1639.

12. Stolz C. A thermodynamical approach to contact wear as application of moving discontinuities. *Archive of Applied Mechanics* 2006; **77**:165–175.
13. Bui HD, Dang Van K, Stolz C. Formulations variationnelles du problme en vitesse pour le solide lastique fragile avec zones endommages. *Comptes Rendus de l'Académie des Sciences*, *Paris* 1981; **292, Ser. II**:251–254.
14. Pradeilles-Duval RM, Stolz C. Mechanical transformations and discontinuities along a moving surface. *Journal of the Mechanics and Physics of Solids* 1995; **43**:91–121.
15. Archard JF. Contact and rubbing of flat surfaces. *Journal of Applied Physics* 1953; **24**:981–988.
16. Goryacheva IG, Rajeev PT, Farris TN. Wear under partial slip contact. *Journal of Tribology* 2001; **129**:848–856.
17. Johansson L. Numerical simulation of contact pressure evolution in fretting. *Journal of Tribology* 1994; **116**: 247–254.
18. Alart P, Curnier A. A mixed formulation for frictional contact problems prone to Newton like solution methods. *Computer Methods in Applied Mechanics and Engineering* 1991; **92**:353–375.
19. Simo JC, Laursen TA. An augmented Lagrangian treatment of contact problems involving friction. *Computers and Structures* 1992; **42**:97–116.
20. Klarbring A. Mathematical programming and augmented Lagrangian methods for frictional contact problems. In *Proceedings of Contact Mechanics International Symposium*, Curnier A (ed.). Presses Polytechniques et Universitaires Romandes, Suisse, 409–422.
21. Laursen TA, Simo JC. A continuum-based finite element formulation for the implicit solution of multibody large deformation frictional contact problems. *International Journal for Numerical Methods in Engineering* 1993; **35**:3451–3485.
22. Klarbring A. Large displacement frictional contact: a continuum framework for finite element discretization. *European Journal of Mechanics A/Solids* 1995; **2**:237–253.
23. Curnier A, He QC, Klarbring A. Continuum mechanics modeling of large deformation contact with friction. In *Contact Mechanics*, Raous M, Jean M, Moreau JJ (eds). Plenum: New York, 1995; 145–158.
24. Wriggers P. Finite element methods for contact problems with friction. *Tribology International* 1996; **29**:651–658.
25. McColl IR, Ding J, Leen SB. Finite element simulation and experimental validation of fretting wear. *Wear* 2004; **256**:1114–1127.
26. Stromberg N. A Newton method for three-dimensional fretting problems. *International Journal of Solids and Structures* 1999; **36**:2075–2090.
27. Costello GA. *Theory of Wire Rope*. Springer: Berlin, 1990.
28. Durvillle D. Modélisation du comportement mécanique des cables métalliques. *European Journal of Computational Mechanics* 1998; **7**:9–22.
29. Agelet de Saracibar C, Chiumenti M. On the numerical modeling of frictional wear phenomena. *Computer Methods in Applied Mechanics and Engineering* 1999; **177**:404–426.
30. Podra P. FE wear simulation of sliding contacts. *Doctoral Thesis*, Royal Institute of Technology, Stockholm, 1997.
31. Podra P, Andersson S. Simulating sliding wear with finite element method. *Tribology International* 1999; **32**:71–81.
32. Oqvist M. Numerical simulations of mild wear using updated geometry with different step size approaches. *Wear* 2001; **249**:6–11.
33. Paulin C, Fouvry S, Meunier C. Finite element modelling of fretting wear surface evolution: application to a Ti-6A1-4V contact. *Wear* 2008; **1–2**:26–36.
34. Madge JJ, Leen SB, Shipway PH. The critical role of fretting wear in the analysis of fretting fatigue. *Wear* 2007; **263**:542–551.
35. Molinari JF, Ortiz M, Radovitzky R, Repetto EA. Finite-element modelling of dry sliding wear in metals. *Engineering Computations* 2001; **18**:592–609.
36. Hattori T, Watanabe T. Fretting fatigue strength estimation considering the fretting wear process. *Tribology International* 2006; **39**:1100–1105.
37. Shillor M, Sofonea M, Touzani R. Quasistatic frictional contact and wear of a beam. *Dynamics of Continuous*, *Discrete and Impulsive Systems* 2000; **8**:201–218.
38. Gu RJ, Kuttler KL, Shillor M. Frictional wear of a thermoelastic beam. *Journal of Mathematical Analysis and Applications* 2000; **242**:212–236.
39. Kim KH, Kim SJ, Yoon KH, Kang HS, Song KN. Fretting wear of laterally supported tube. *Wear* 2001; **250**:535–543.
40. Kim HK, Lee YH. Wear depth model for thin tubes with supports. *Wear* 2007; **263**:532–541.
41. Ben Dhia H. Multiscale mechanical problems: the Arlequin method. *Comptes Rendus de l'Académie des Sciences Série IIb* 1998; **326**:899–904.
42. Ben Dhia H. Numerical modeling of multiscale mechanical problems: the Arlequin method. *ECCM'99*, Munchen, 1999.
43. Ben Dhia H, Rateau G. Application of the Arlequin method to some structures with defects. *European Journal of Computational Mechanics* 2002; **11**:291–304.
44. Ben Dhia H, Rateau G. The Arlequin method as a flexible engineering design tool. *International Journal for Numerical Methods in Engineering* 2005; **62**:1442–1462.
45. Ben Dhia H, Zarroug M. Hybrid frictional contact particles-in elements. *European Journal of Computational Mechanics* 2002; **11**:417–430.

46. Ben Dhia H, Zammali C. Level-sets, placement and velocity-based Lagrangian formulation of impact problems. *International Journal for Numerical Methods in Engineering* 2007; **69**:2711–2735.
47. Hallquist JQ, Goudreau GL, Benson DJ. Sliding interface with contact-impact in large-scale Lagrangian computations. *Computer Methods in Applied Mechanics and Engineering* 1985; **51**:107–137.
48. Ben Dhia H, Durville D. Calembour: an implicit method based on an enriched kinematical thin-plate model for sheet-metal forming simulation. *Journal of Materials Processing Technology* (*Source*: *Congress NUMISHEET '93*: *International Conference on Numerical Simulation of 3-D Sheet Metal Forming Processes No. 2*, *Isehara*, *Japan* (31/08/1993)) 1995; **50**:70–80.
49. Ben Dhia H. Further insights by theoretical investigations of the multiscale Arlequin method. *International Journal for Multiscale Computational Engineering* 2008; **6**:215–232.
50. Xiao SP, Belytschko T. A bridging domain method for coupling continua with molecular dynamics. *Computer Methods in Applied Mechanics and Engineering* 2004; **193**:1645–1669.
51. Bauman P, Ben Dhia H, Elkhodja N, Prudhomme S. On the application of the Arlequin method to the coupling of particle and continuum models. *Computer Methods in Applied Mechanics and Engineering* 2008; **42**:511–530.
52. Prudhomme S, Chamoin L, Ben Dhia H, Bauman P. An adaptive strategy for the control of modeling error in two-dimensional atomistic to continuum coupling simulations. *Computer Methods in Applied Mechanics and Engineering* 2009; **42**:1887–1901.
53. Ben Dhia H, Zarroug M. Contact in the Arlequin framework. *Contact Mechanics* (*CMIS*, *2001*). Kluwer Publishers: Dordrecht, 2002; 403–410.
54. Osher S, Sethian JA. Fronts propagating with curvature-dependent speed: algorithms based on Hamilton Jacobi formulations. *Journal of Computational Physics* 1988; **79**:12–49.
55. Szabó B, Babuska I. *Finite Element Analysis*. Wiley: New York, 1991.
56. Hattori T, Nakamura M, Watanabe T. Simulation of fretting-fatigue life by using stress-singularity parameters and fracture mechanics. *Tribology International* 2003; **36**:87–97.